Available online at www.sciencedirect.com
ScienceDirect
Journal of Power Sources 168 (2007) 369–378
JOURNAL OF POWER SOURCES
www.elsevier.com/locate/jpowsour

Micro-scale modelling of solid oxide fuel cells with micro-structurally graded electrodes

Meng Ni, Michael K.H. Leung *, Dennis Y.C. Leung

Department of Mechanical Engineering, The University of Hong Kong, Pokfulam Road, Hong Kong, China

Received 30 December 2006; received in revised form 5 March 2007; accepted 5 March 2007
Available online 12 March 2007

Abstract

A mathematical model was developed for modelling the performance of solid oxide fuel cell (SOFC) with functionally graded electrodes at the micro-scale level. The model considered all forms of overpotentials and was able to capture the coupled electrochemical reactions and mass transfer involved in the SOFC operation. The model was validated by comparing the simulation results with experimental data from the literature. Additional modelling analyses were conducted to gain better understanding of the SOFC working mechanisms at the micro-scale level and to quantify the performance of micro-structurally graded SOFC. It was found that micro-structural grading could significantly enhance the gas transport but had negligible effects on the ohmic and activation overpotentials, especially for thick electrodes. However, for thin electrodes with large particles, too much grading should be avoided as the increased activation overpotentials may result in higher overall overpotentials at a medium or low current density. Among all the cases tested in the present study, the micro-structurally graded SOFC showed significantly higher power density than conventional SOFC of uniform porosity and particle size. The difference between micro-structurally graded SOFC and conventional SOFC is more pronounced for smaller electrode–electrolyte (EE) interfacial particles. Particle size grading is generally more effective than porosity grading and it can increase the maximum power density by one-fold in comparison with conventional SOFC. The present study reveals the working mechanisms of SOFC at the micro-scale level and demonstrates the promise of the use of micro-structural grading to enhance the SOFC performance.

Keywords: SOFC; Functionally-graded electrodes; Multi-component mass transfer; Porous media; Parametric analyses

1. Introduction

Solid oxide fuel cells (SOFCs), which are efficient, tolerant of impurities, and flexible in fuel choices, will play an important role in the next generation of energy technology [1–3]. In order to further enhance its energy conversion efficiency, efforts have been made in developing new materials and designing novel geometries. Hwang et al. [4] developed a numerical model to investigate the characteristics of a mono-block-layer-built (MOLB) SOFC and they found that the MOLB-SOFC had a higher fuel/oxidant utilization than the planar SOFC. Ramakrishna et al. [5] performed numerical analyses and proposed an innovative thin-walled geometry to improve the power density of SOFC. More recently, a novel 3-D SOFC was developed by Koh et al. [6] to increase the volumetric power density by increasing the volumetric surface areas of the electrodes. The philosophy of these studies is to optimise the fuel/reactant flow field at the macro-scale level so as to improve the cell performance.

Functionally graded electrodes (FGE) have been applied to SOFC in the recent years and offered potentials to enhance the SOFC performance at the micro-scale level [7–10]. Grading can be classified into three ways: (1) composition grading, (2) particle size grading, and (3) porosity grading. The porosity grading and particle size grading are two forms of micro-structural grading. The aim of grading is to optimise the electronic/ionic conductivity, to increase the electrochemical reactivity of the electrode, or to enhance the gas transport. Despite some experimental works available in the literature, the modelling studies on FGE are limited. Schneider et al. [10] investigated the percolation effects in composition graded SOFC electrodes with Kirchhoff's current law. It was found that the graded electrodes with varying composition did not perform significantly better than the non-graded electrode but the percolation was improved. Greene et al. [11] developed a macro-scale numerical

* Corresponding author. Tel.: +852 2859 2628; fax: +852 2858 5414.
E-mail address: mkhleung@hku.hk (M.K.H. Leung).

0378-7753/$ – see front matter © 2007 Elsevier B.V. All rights reserved.
doi:10.1016/j.jpowsour.2007.03.005

model to investigate the mass transport phenomena of porosity graded SOFC electrodes. The effects of porosity change on the concentration and ohmic overpotentials were considered in their macro-scale model but the activation overpotential was treated as a property independent of the porosity as the electrochemical reactions were assumed to occur merely at the electrode–electrolyte (EE) interface. With a uniform pore size along the depth, an enhanced SOFC performance (8.7% improvement) was observed for the porosity-graded electrodes due to the reduced transport resistance [11].

Despite the abovementioned investigations, the studies on micro-structurally graded SOFC are insufficient and its mechanisms are not well understood. First, the literature is lacking detailed modelling of the particle size graded SOFC. In addition, the existing study on porosity graded SOFC at the macro-scale level is insufficient to provide details to explain how porosity grading affects the SOFC performance. The present study aims to analyse the performance of micro-structurally graded SOFC by micro-scale modelling. The porosity grading and particle size grading have been investigated and their potentials for use in SOFC have been evaluated by comparison with non-graded SOFC. The model developed is able to predict the micro-level distributions of gas concentration, current densities, and electrochemical reactions along the electrode depth as well as the macro-level SOFC performance. The results presented in this paper are valuable for design optimisation of SOFC.

2. Model development

2.1. Working mechanisms of SOFC

The coupled electrochemical reaction and mass transfer in a non-graded composite anode are illustrated in Fig. 1. The reaction processes can be summarized as: (1) transport of reactant (H_2) to the reaction sites through the pores of the anode and transport of O^{2-} from the electrolyte to the reaction sites through the ionic conducting particles; (2) electrochemical reaction of H_2 and O^{2-} to form H_2O and electrons at the active sites; (3) transport of electrons from the active sites to the current collector through the electronic conducting particles and transport of the H_2O product to the anode surface via the pores of the anode.

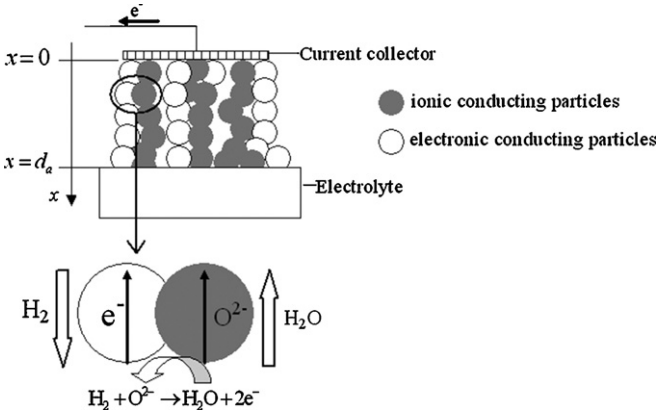

Fig. 1. Schematic of the composite anode of a SOFC, consisting of both electronic conducting particles and ionic conducting particles.

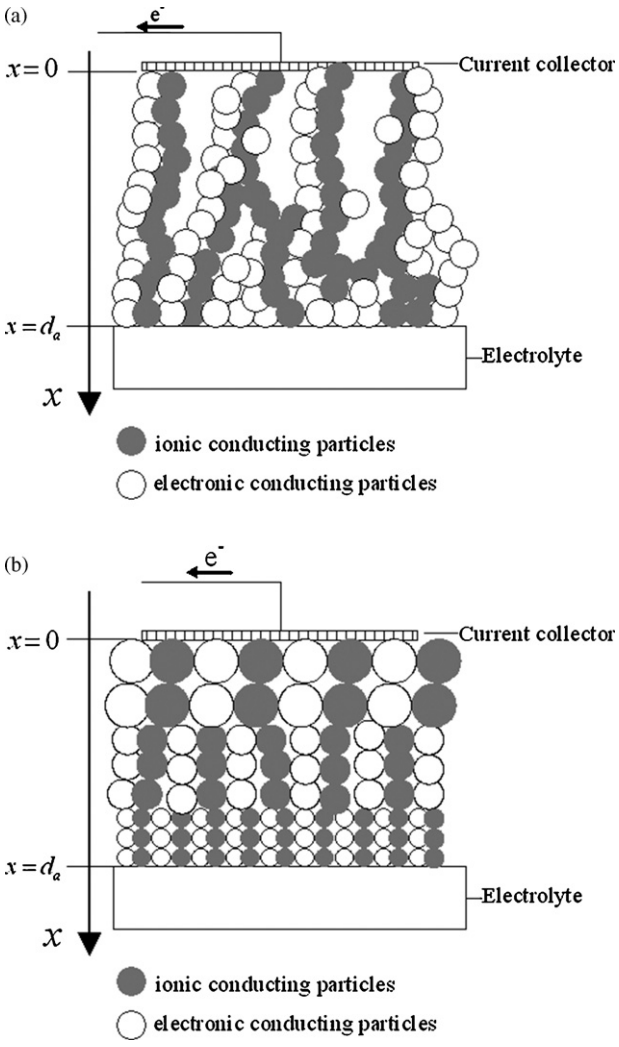

Fig. 2. Schematic of the functionally graded anode: (a) porosity grading with constant particle size; (b) particle size grading with constant porosity.

Compared with a conventional non-graded electrode (Fig. 1), a graded electrode can be formed by either one of the two different types of micro-structural grading, namely porosity grading and particle size grading. Fig. 2 shows the two types of grading done on an anode. Both porosity and particle size can vary along the depth of the anode, from a larger value at the anode surface to a smaller value at the EE interface. A graded cathode can be formed in similar manners.

2.2. The anode

Charge balance in the electronic/ionic conducting particles can be written as

$$\nabla \cdot J_{e,a} = -S_V J_{n,a} = -\nabla \cdot J_{i,a} \quad (1)$$

where $J_{e,a}$ and $J_{i,a}$ is the current density (A m^{-2}) in the electronic and ionic conductors, respectively; S_V the electrochemically active internal surface area per unit volume of the porous anode (m^2 m^{-3}), which depends on the electrode depth in an FGE; and $J_{n,a}$ is the transfer current per unit area of reactive surface (A m^{-2}).

The active surface area (S_V) can be calculated with the method based on the binary random packing theories [12–15]

$$S_V = \pi \sin^2\theta r_e^2 n_t n_e n_i \frac{Z_e Z_i}{6} P_e P_i \quad (2)$$

where θ is the contact angle between the electronic and ionic conductors; r_e the radius of the electronic conductors; n_t the total number of particles per unit volume; n_e and n_i the number fractions of electronic and ionic conductors, respectively; Z_e and Z_i the coordination numbers of electronic and ionic conductors, respectively; P_e the probability of electronic conductors connected with the porous media; and P_i is the probability of ionic conductors connected with the porous media.

The total number of particles per unit volume, depending on porosity ε and particle sizes (radii r_e and r_i for electronic conductors and ionic conductors, respectively), can be determined according to [14],

$$n_t = \frac{1-\varepsilon}{(4/3)\pi r_e^3[n_e + (1-n_e)(r_i/r_e)^3]} \quad (3)$$

Other parameters used in Eq. (2) can be calculated by the same way with Costamagna et al. [13] and Chan and Xia [12]. In the present study, r_e is assumed equal to r_i at the same electrode depth.

The transfer current density $J_{n,a}$ can be determined by the generalized Butler Volmer equation [13],

$$J_{n,a} = J_{0,a}^{ref}\left\{\frac{P_{H_2}}{P_{H_2}^0}\exp\left(\frac{\alpha z F\eta_a}{RT}\right) - \frac{P_{H_2O}}{P_{H_2O}^0}\exp\left(-\frac{(1-\alpha)zF\eta_a}{RT}\right)\right\} \quad (4)$$

where J_0^{ref} is the reference exchange current density; P_{H_2O} and $P_{H_2O}^0$ the partial pressures of H_2O within the porous anode and at the anode surface, respectively; similarly, P_{H_2} and $P_{H_2}^0$ the partial pressures of H_2; α the charge transfer coefficient, which is 0.5 for SOFC [16]; z the number of charges involved per reaction; and η_a is the overpotential in anode. The value of η_a is defined as [12,13]

$$\eta_a = (\phi_{e,a}^0 - \phi_{i,a}^0) - (\phi_{e,a} - \phi_{i,a}) \quad (5)$$

where $\phi_{i,a}$ and $\phi_{e,a}$ denote the ionic and electronic potentials, respectively; the superscript 0 represents the equilibrium condition.

The electronic and ionic potentials can be obtained by applying Ohm's law,

$$\nabla\cdot\phi_{e,a} = \rho_{e,a}^{eff} J_{e,a} \quad \text{and} \quad \nabla\cdot\phi_{i,a} = \rho_{i,a}^{eff} J_{i,a} \quad (6)$$

where ρ^{eff} is the effective resistivity (Ω m); J the current density; and the subscripts i and e represents, respectively, the ionic and electronic conductors. The effective resistivity of electronic and ionic conductors can be determined by [14]

$$\rho_{e,a}^{eff} = \frac{\xi}{\Phi(1-\varepsilon)\sigma_{e,a}} \quad \text{and} \quad \rho_{i,a}^{eff} = \frac{\xi}{(1-\Phi)(1-\varepsilon)\sigma_{i,a}} \quad (7)$$

where Φ is the volume fraction of the electronic conducting particles; ξ the tortuosity of the electrode; $\sigma_{e,a}$ and $\sigma_{i,a}$ are the conductivities of solid electronic conductor and ionic conductors, respectively.

The first and second derivatives of η_a can be written as

$$\frac{d\eta_a}{dx} = \rho_{i,a}^{eff} J_{i,a} - \rho_{e,a}^{eff} J_{e,a} \quad (8)$$

and

$$\frac{d^2\eta_a}{dx^2} = \rho_{i,a}^{eff}\frac{dJ_{i,a}}{dx} - \rho_{e,a}^{eff}\frac{dJ_{e,a}}{dx} = S_V J_{n,a}(\rho_{i,a}^{eff} + \rho_{e,a}^{eff}) = S_V J_{0,a}^{ref}(\rho_{i,a}^{eff} + \rho_{e,a}^{eff})\left\{\frac{P_{H_2}}{P_{H_2}^0}\exp\left(\frac{\alpha z F\eta_a}{RT}\right) - \frac{P_{H_2O}}{P_{H_2O}^0}\exp\left(-\frac{(1-\alpha)zF\eta_a}{RT}\right)\right\} \quad (9)$$

At the anode surface, $J_{i,a}=0$ and $J_{e,a}=J_{total}$. At the EE interface, $J_{i,a}=J_{total}$ and $J_{e,a}=0$. Therefore, the two boundary conditions for the above second order differential equation (Eq. (9)) can be written as

$$x=0,\ \left.\frac{d\eta_a}{dx}\right|_{x=0} = -\rho_{e,a}^{eff} J_{total} \quad \text{and} \quad x=d_a,\ \left.\frac{d\eta_a}{dx}\right|_{x=d_a} = \rho_{i,a}^{eff} J_{total} \quad (10)$$

In the steady state, the conservation of gas species can be written as

$$\nabla\cdot N_i = R_i \quad (11)$$

where N_i denotes the rate of mass transport (mol m^{-2} s^{-1}) and R_i represents the rate of reaction inside the porous electrode (mol m^{-3} s^{-1}). The rates of reaction for H_2O and H_2 can be expressed as $R_{H_2} = -S_V J_{n,a}/2F$ and $R_{H_2O} = S_V J_{n,a}/2F$, respectively.

The mass transfer process of H_2 in the porous electrode is by means of diffusion. Considering both Knudsen diffusion and molecular diffusion, the mass flux of hydrogen can be determined by the Dusty Gas Model (DGM) as

$$N_{H_2} = -\frac{P}{RT}\left(\frac{1}{D_{H_2,k}^{eff}} + \frac{1-\alpha y_{H_2}}{D_{H_2O-H_2}^{eff}}\right)^{-1}\frac{dy_{H_2}}{dx} \quad (12)$$

where $\alpha = 1 - \sqrt{M_{H_2}/M_{H_2O}}$; M_{H_2} and M_{H_2O} the molecular weights of H_2 and H_2O, respectively; and $D_{H_2,k}^{eff}$ and $D_{H_2O-H_2}^{eff}$ are the Knudsen diffusion coefficient of H_2 and the binary diffusion coefficient of H_2–H_2O mixture, respectively. The calculation of the abovementioned diffusion coefficients, which are functions of the microstructures of the electrodes, can be found in references [17,18]. The important pore radius can be obtained by the expression developed by Nam and Jeon [19] as

$$r_p = \frac{2}{3}\frac{r_e\varepsilon}{1-\varepsilon} \quad (13)$$

Substituting Eq. (12) into Eq. (11), the controlling equation for H_2 diffusion becomes

$$\frac{d^2 y_{H_2}}{dx^2} + \frac{\alpha}{D^{eff}_{H_2O-H_2}}\left(\frac{1}{D^{eff}_{H_2,k}} + \frac{1-\alpha y_{H_2}}{D^{eff}_{H_2O-H_2}}\right)^{-1}\left(\frac{dy_{H_2}}{dx}\right)^2 - \frac{S_V J_{n,a} RT}{2FP}\left(\frac{1}{D^{eff}_{H_2,k}} + \frac{1-\alpha y_{H_2}}{D^{eff}_{H_2O-H_2}}\right) = 0 \quad (14)$$

The boundary conditions for Eq. (14) are given below

$$y_{H_2}\Big| = y^0_{H_2}\ ;\ \frac{dy_{H_2}}{dx}\Big|_{x=0} = -\frac{RTJ_{total}}{2FP}\left(\frac{1}{D^{eff}_{H_2,k}} + \frac{1-\alpha y_{H_2}}{D^{eff}_{H_2O-H_2}}\right) \quad (15)$$

In the abovementioned equations, the gas molar fraction, gas diffusion coefficients, electronic/ionic current density, reaction rate, and the overpotential are dependent of depth x. Due to the complicated phenomena involved, an iterative scheme is used to solve the non-linear equations. The iterative computation is successful if a convergence is obtained. After obtaining the distributions of species concentration, current densities, and overpotentials, the overall electrode overpotential can be determined [13],

$$\eta_{t,a} = (\phi^0_{e,a} - \phi^0_{i,a}) - (\phi_{e,a(x=0)} - \phi_{i,a(x=d_a)}) \quad (16)$$

2.3. The cathode

Similar to the anode, the coupled electrochemical reactions and transport phenomena at the SOFC cathode can be determined,

$$\frac{d^2\eta_c}{dx^2} = \rho^{eff}_{i,c}\frac{dJ_{i,c}}{dx} - \rho^{eff}_{e,c}\frac{dJ_{e,c}}{dx} = S_V J_{n,c}(\rho^{eff}_{i,c} + \rho^{eff}_{e,c}) = S_V J^{ref}_{0,c}(\rho^{eff}_{i,c} + \rho^{eff}_{e,c})\left\{\frac{P_{O_2}}{P^0_{O_2}}\exp\left(\frac{\alpha z F\eta_c}{RT}\right) - \exp\left(-\frac{(1-\alpha)\,zF\eta_c}{RT}\right)\right\} \quad (17)$$

and

$$\nabla\cdot J_{e,c} = -S_V J_{n,c} = -S_V J^{ref}_{0,c}\left\{\frac{P_{O_2}}{P^0_{O_2}}\exp\left(\frac{\alpha z F\eta_c}{RT}\right) - \exp\left(-\frac{(1-\alpha)zF\eta_c}{RT}\right)\right\} \quad (18)$$

Similar to the anode, the boundary conditions for Eqs. (17) and (18) are

$$x = 0,\ J_{e,c} = J_{total},\ \frac{d\eta_c}{dx} = -\rho^{eff}_{e,c}J_{total};$$
$$x = d_c,\ J_{i,c} = J_{total},\ \frac{d\eta_c}{dx} = \rho^{eff}_{i,c}J_{total} \quad (19)$$

The transport of O_2 can be described by the self-diffusion mechanism [20],

$$\frac{dP_{O_2}}{dx} = -\frac{RTJ_{e,c}}{4FD^{eff}_{O_2}P_c}(P_c - \delta_{O_2}P_{O_2}) \quad (20)$$

and

$$\delta_{O_2} = \frac{D^{eff}_{O_2,k}}{D^{eff}_{O_2,k} + D^{eff}_{O_2-N_2}} \quad (21)$$

The boundary condition for transport of O_2 (Eq. (20)) is $P_{O_2} = P^0_{O_2}$ at $x = 0$. The cathode total overpotential can be obtained as [13]

$$\eta_{t,c} = (\phi^0_{i,c} - \phi^0_{e,c}) - (\phi_{i,c(x=d_c)} - \phi_{e,c(x=0)}) \quad (22)$$

2.4. The electrolyte

The dense electrolyte is typically made of yttrial-stabilized zirconia (YSZ) and is used to conduct O^{2-}. The overpotential of the dense electrolyte can be determined by Ohm's law,

$$\eta_e = J_{total}R_eL \quad (23)$$

where R_e and L are the resistivity (Ω m) and thickness (m) of the electrolyte, respectively.

3. Model validation

In this section, the model as described in the previous section is validated by comparison with experimental data. The values of the input parameters for subsequent simulation and analyses are summarized in Table 1 [12,13,16,21,22], unless otherwise stated.

Table 1
Values of input parameters used in the present model

Parameter	Value
Temperature, T (K)	1073
Pressure, P (atm)	1.0
Reference anode exchange current density, $J^{ref}_{0,a}$ (A m^{-2})	4000.0 [21]
Reference cathode exchange current density, $J^{ref}_{0,c}$ (A m^{-2})	1300.0 [21]
Anode thickness, d_a (m)	500×10^{-6}
Cathode thickness, d_c (m)	50×10^{-6}
Electrolyte thickness, L (m)	50×10^{-6}
Conductivity of electronic conductor of anode, $\sigma_{e,a}$ (S m^{-1})	2×10^6 [12,13]
Conductivity of electronic conductor of cathode, $\sigma_{e,c}$ (S m^{-1})	1×10^4 [22]
Conductivity of ionic conductor, $\sigma_{i,a}$,$\sigma_{i,c}$ (S m^{-1})	$3.44\times10^4\exp(-10300/T)$ [12,13]
Electrode tortuosity, ξ	4.5 [12,13]
Volume fraction of electronic conductor, Φ	0.4 [12,13]
Electrode porosity, ε[a]	0.3 [12,13]
Particle size, r_e, r_i (m)[a]	0.5×10^{-6} [16]

[a] *Note:* The values of porosity and particle size are used as typical microstructure parameters. Other values for FGE and for comparative analyses are also used and specified in the text.

Jiang et al. [23] described their laboratory set-up and experimental test procedures in detail and, therefore, their work was selected for model validation. In their experiments, both pure Ni and Ni-YSZ cermet anodes with different YSZ loadings were tested. The volume percentages of the impregnated YSZ in the anode were 17 vol.% and 21 vol.% with YSZ loadings of 2.7 mg cm^{-2} and 4.0 mg cm^{-2}, respectively. In the sample preparation, an anode was deposited on a 1-mm YSZ electrolyte. The thickness of the anode was about 30 μm and its porosity was 30%. The tests were conducted under a constant pressure of 1 atmosphere (atm), H_2 molar fraction of 97% (3% H_2O), and temperature ranging from 973 K to 1173 K. The performance of the pure Ni and Ni-YSZ cermet anodes were characterized by polarization and electrochemical impedance spectroscopy (EIS). Fig. 3(a) shows the dependence of anode overpotential on current density at different YSZ loadings. A good agreement between the theoretical simulation and the experimental data is found. The Ni-YSZ cermet anodes have a lower overpotential than the pure Ni anode. It is because the electrochemical reactions are extended from the EE interface to the inner Ni-YSZ electrode, resulting in an enhanced electrode reactivity. Fig. 3(b) shows the effect of operating temperature on the overpotential of the cermet anode with 2.7 mg cm^{-2} YSZ loading. The anode performance increases with increasing temperature due to the enhanced ion conduction. Again, the simulated results agree reasonably well with the experimental data by Jiang et al. [23].

In the second simulation, the *J–V* characteristics of the SOFC were simulated and compared with the experimental data by Kim et al. [24]. In Kim et al.'s experiments, the anode, cathode, and the electrolyte were made of Ni-YSZ, YSZ, and $La_{0.8}Sr_{0.2}MnO_3$-YSZ, with thickness about 1.2 mm, 30 μm, and 7 μm, respectively. Experiments were conducted at a pressure of 1 atm, temperature of 1073 K, and a H_2 molar fraction of 97% (3% H_2O). The measured *J–V* data were compared with the theoretical simulation results as plotted in Fig. 3(c). Again, a good agreement between simulation results and experimental data was found. Fig. 3(a–c) serve as a thorough validation of the present model.

4. Results and discussion

In the following analyses, a conventional non-graded SOFC and a micro-structurally graded SOFC were studied for their electrochemical performance. From the previous studies, SOFC electrode particles having radii ranging from 0.012 μm to 5.0 μm have been reported [25–27]. For electrodes made from spherical particles, the achievable porosity ranges from 0.3 to 0.7. For a porosity less than 0.3, the extent of overlap between spherical particles increases with decreasing porosity, causing the active surface area to decrease considerably with decreasing porosity [28–30]. For a porosity higher than 0.7, the electrode will suffer from poor particle connectivity, poor percolation, and thus poor performance [30,31]. Therefore, for electrodes consisting of spherical particles, porosity between 0.3 and 0.7 is regarded as a practical range. Without losing generality, the most favourable anode-supported configuration with thick anode and thin cathode/electrolyte is considered in this study.

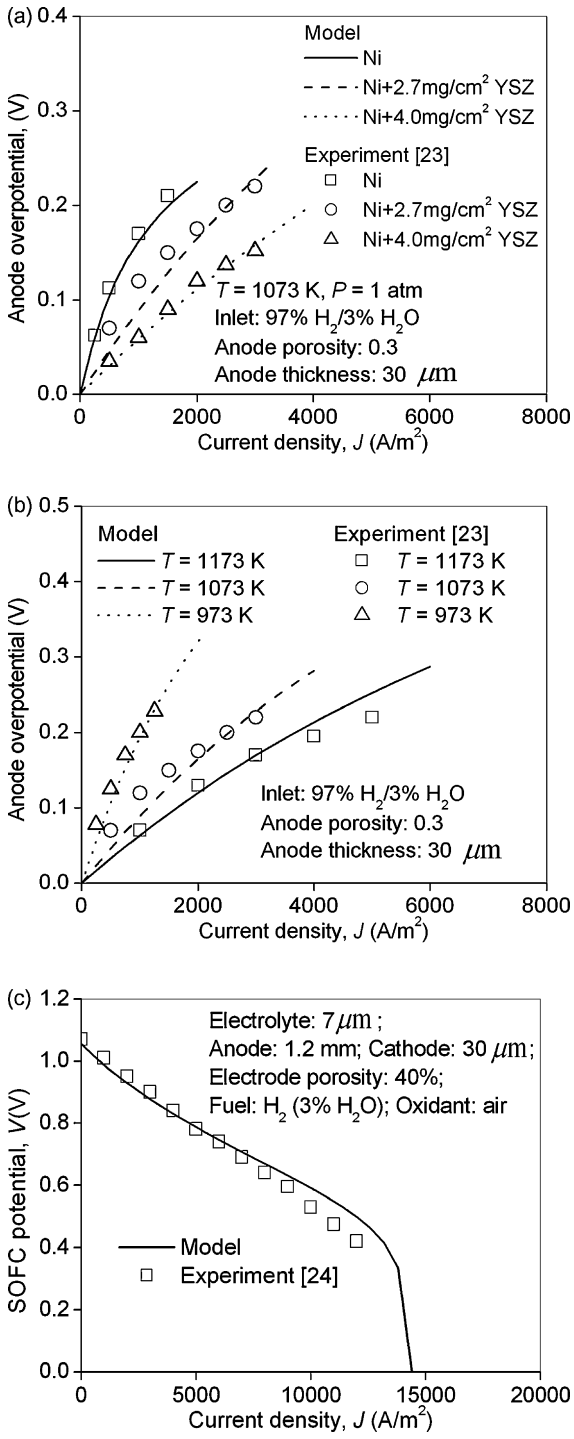

Fig. 3. Comparison between simulation results and experimental data from literature for model validation: (a) anode overpotential at different YSZ loadings; (b) anode overpotential at different temperatures; and (c) *J–V* characteristics of a planar SOFC.

4.1. Current density and gas composition distribution in electrodes

In this section, the distributions of electronic/ionic current density and gas composition along the electrode depth were studied at the typical operating current density of 10,000 A m^{-2}. Fig. 4(a) shows the distributions of electronic/ionic current den-

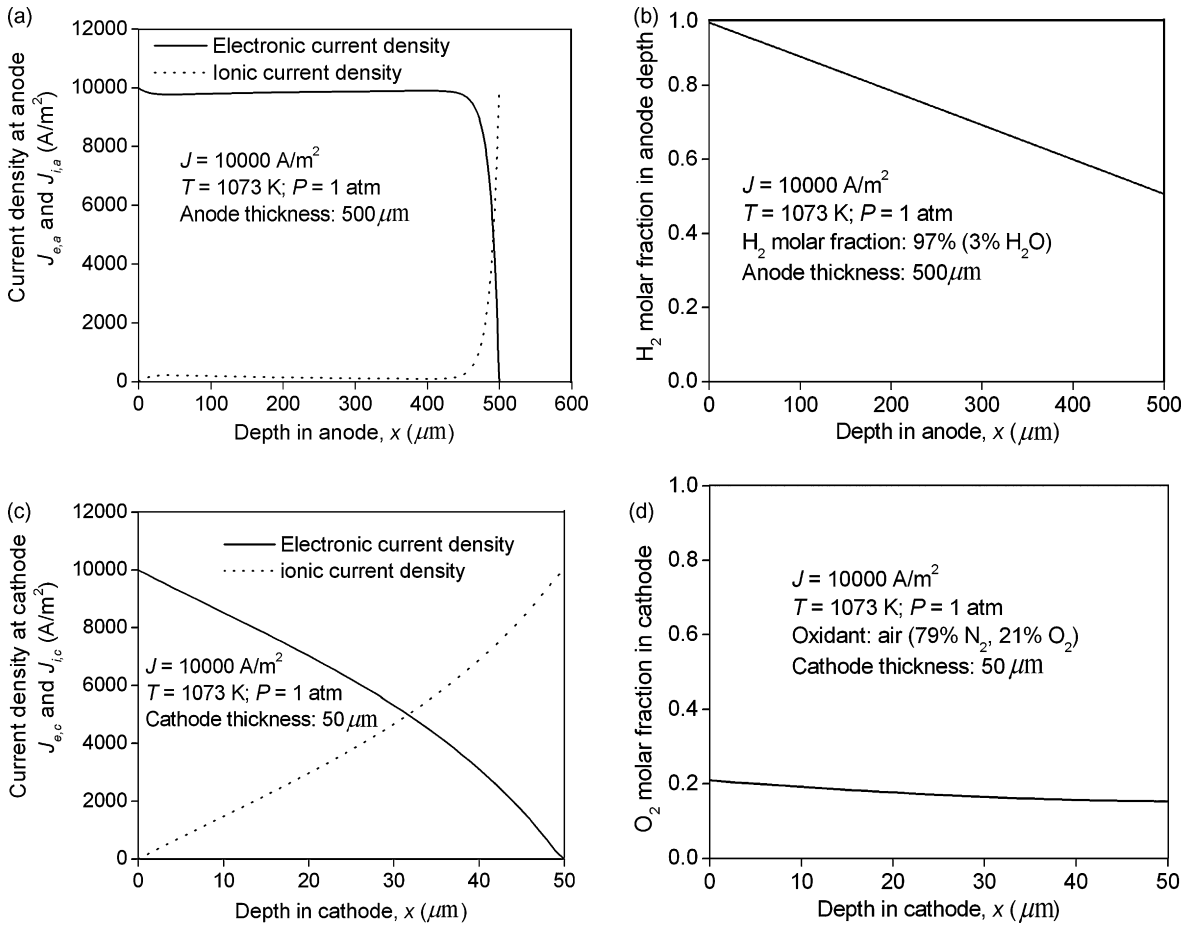

Fig. 4. Current density and gas composition distribution along electrode depth: (a) electronic and ionic current density distribution in anode; (b) H_2 molar fraction distribution in anode; (c) electronic and ionic current density distribution in cathode; and (d) O_2 molar fraction distribution in cathode.

sity in porous anode. The electronic current density increases from 0 at the EE interface ($x = 500\,\mu m$) to the maximum ($10{,}000\ A\ m^{-2}$) at the anode surface ($x = 0$), where electrons are collected. The ionic current density shows a reverse trend of electronic current density. The sharp change of electronic/ionic current density at the EE interface indicates that most of the electrochemical reactions occur there. It is because the effective ionic conductivity is much lower than that of electronic conductivity. Fig. 4(b) shows the distribution of H_2 molar fraction in the anode region. The concentration of H_2 decreases considerably from the anode surface towards the EE interface, indicating the importance of gas transport in the thick anode (500 μm). The electronic/ionic current density distribution in the porous cathode is shown in Fig. 4(c). The steady changes in electronic/ionic current density indicate that electrochemical reactions take place throughout the thin cathode (50 μm thick). In addition, the thin cathode shows a very low mass transfer resistance, as can be seen from Fig. 4(d).

4.2. Effect of electrode microstructure on electrode performance

In order to better understand the effect of micro-structural grading, it is important to understand how the micro-structural parameters affect the electrode performance. In this section, the important electrode porosity and particle size are analysed.

Fig. 5 shows the effect of particle size on the electrode overpotential. For both anode and cathode, optimal particle sizes of about 1.0 μm and 0.3 μm are found. In general, the smaller the particle size, the larger the volumetric reactive surface area (indicated by Eqs. (2) and (3)). Therefore, reducing particle

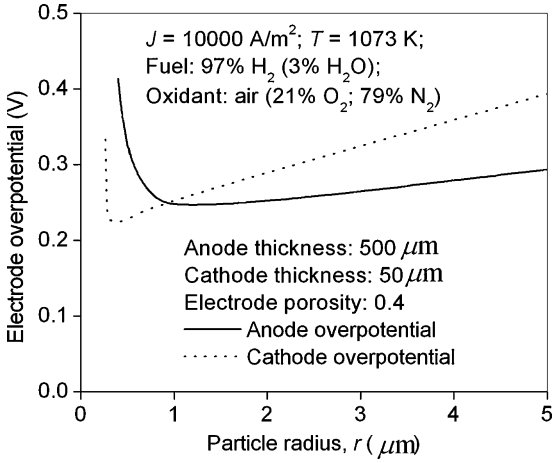

Fig. 5. Effect of particle size on electrode overpotential.

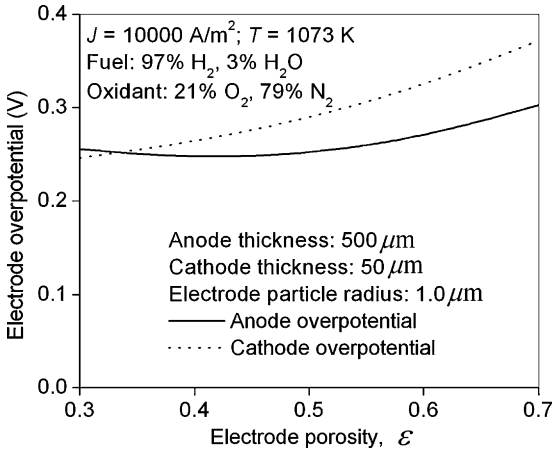

Fig. 6. Effect of porosity on electrode overpotential.

size can increase the electrode reactivity and thus reduces the electrode activation overpotential. However, when the particle size is too small, the reactant concentration at the reactive sites will approach to zero and thus the concentration overpotential will increase considerably. As the anode in an anode-supported SOFC is much thicker than the cathode, the optimal particle size of the anode is larger than that of the cathode.

Similarly, the effect of electrode porosity is shown in Fig. 6. An optimal porosity of about 0.4 is found for the thick anode. Reducing porosity can reduce the ohmic overpotential, as more solid particles are available to facilitate the transport of electronic/ionic charges. In addition, the activation overpotential is also reduced with decreasing porosity due to the increase in reactive surface area. However, the concentration overpotential of the thick anode increases with decreasing porosity since less space is available for gas transport. The combined effects of porosity on ohmic, activation, and concentration overpotentials for minimisation of the overall overpotential result in an optimal porosity for the anode. For comparison, the cathode overpotential increases monotonically with the increasing porosity. It is because the gas transport does not reach its limit in the thin cathode of an anode-supported SOFC.

4.3. SOFC with micro-structurally graded electrodes

The power density and the electrode overpotentials of SOFC with conventional non-graded electrodes and SOFC with porosity/particle size graded electrodes are compared in Figs. 7–9. As a non-graded SOFC can hardly be operated with particle size less than 0.3 μm due to the large anode concentration overpotential (Fig. 5), a linear grading in particle size in the range from 0.3 μm

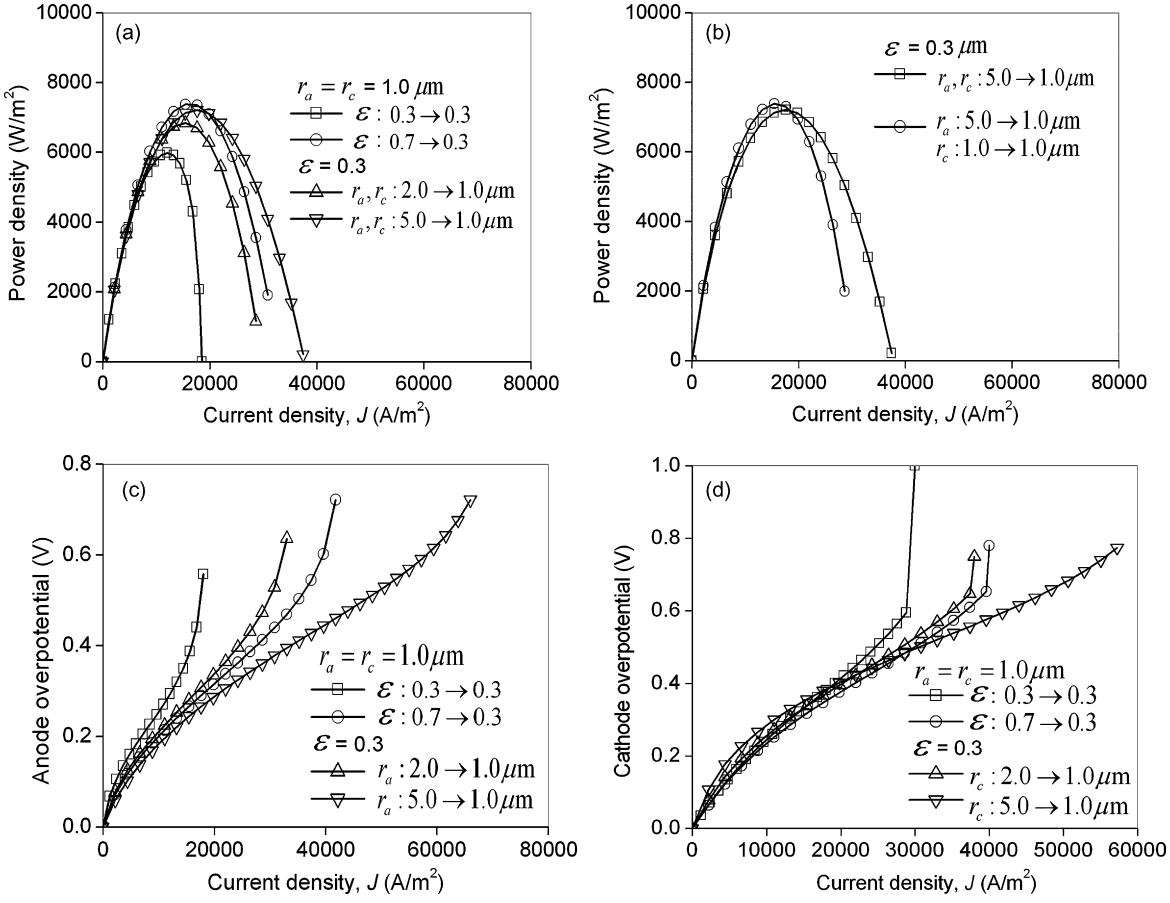

Fig. 7. Comparison of SOFCs with or without FGEs, the particle radius at the EE interface is 1.0 μm: (a) power densities of non-graded SOFC and SOFCs with grading in both electrodes; (b) power densities of SOFC with particle size grading in both electrodes and in one electrode only; (c) anode overpotential; and (d) cathode overpotential.

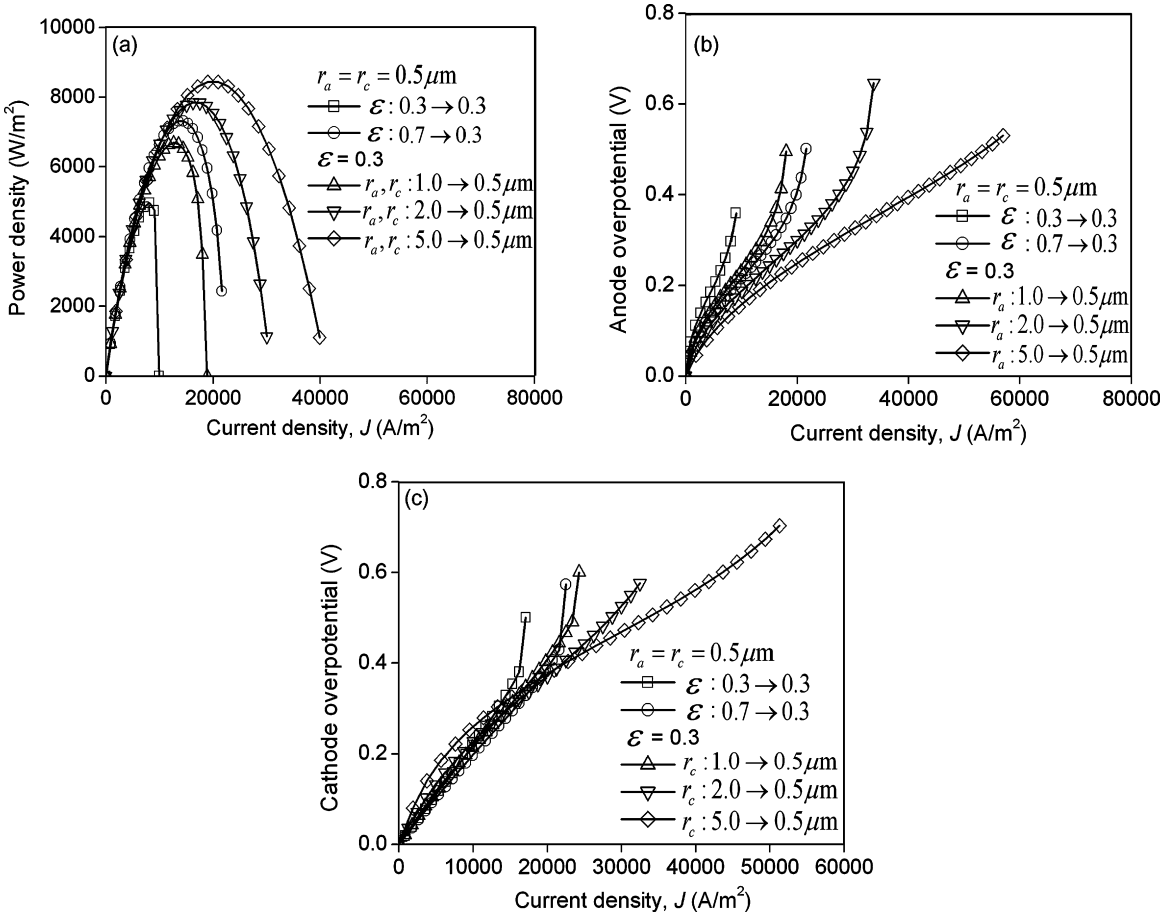

Fig. 8. Comparison of SOFCs with or without FGEs, the EE interfacial particle radius is 0.5 μm: (a) power density; (b) anode overpotential; and (c) cathode overpotential.

to 5.0 μm is studied. In addition, a linear grading of porosity in the range from 0.3 to 0.7 is also employed. In the present study, grading means that the particle size or porosity increases linearly from the EE interface to the electrode surface. As the grading of electrode does not change the performance of electrolyte, the electrolyte ohmic overpotentials are not presented in this paper.

Fig. 7 shows the power density and electrode overpotential of SOFCs with large particle size (1.0 μm) at the EE interface. The maximum power density of a SOFC with porosity-graded electrodes is found to be 23% higher than that of a non-graded SOFC (Fig. 7(a)). Grading of electrode porosity can significantly reduce the mass transfer resistance, but also reduce the volumetric reactive surface area (Eqs. (2) and (3)), and effective electronic/ionic conductivity (Eq. (7)). As the electronic conductivity is several orders of magnitude higher than the ionic conductivity, the ohmic overpotential is primarily caused by the resistance to the ionic current, which mainly occurs at a thin layer close to the EE interface. In addition, the activation overpotentials also mainly take place near the EE interface. For a porosity-graded thick electrode, the porosity does not vary much in the active thin layer. Thus, the ohmic and activation overpotential are insensitive to the porosity grading, especially for thick electrodes. As a result, the porosity-graded electrodes show smaller overpotential than non-graded electrodes (Fig. 7(c and d)). In a previous study conducted by Greene et al. [11], the maximum power density of a porosity graded SOFC is only about 8.7% higher than that of a non-graded SOFC. There is a difference between the present study and Greene et al. [11] due to the overestimation of the ohmic overpotential in Greene et al.'s study. Their macro-scale model cannot predict the distribution of ionic current density and thus they consider the ohmic overpotential to occur throughout the electrode, resulting in an ohmic overpotential higher than the actual value. The present micro-scale model can predict more precisely the performance of SOFC with micro-structurally graded electrodes. Compared with porosity grading, the particle size grading shows comparable performance. In addition, the larger the extent of the anode particle size grading, the lower the anode overpotential, and thus the better the SOFC performance. The grading in cathode can also reduce the mass transport resistance and thus shift the limiting current density to a larger value (Fig. 7(d)). Unlike porosity grading, particle size grading does not change the ohmic overpotential. However, when the particle size grading is too radical for the thin cathode (r_c: 5.0 μm → 10 μm), the activation overpotential will become more important at low to medium current density, as can be seen from Fig. 7(d). Under these circumstances, too much grading of the cathode may result in a poorer

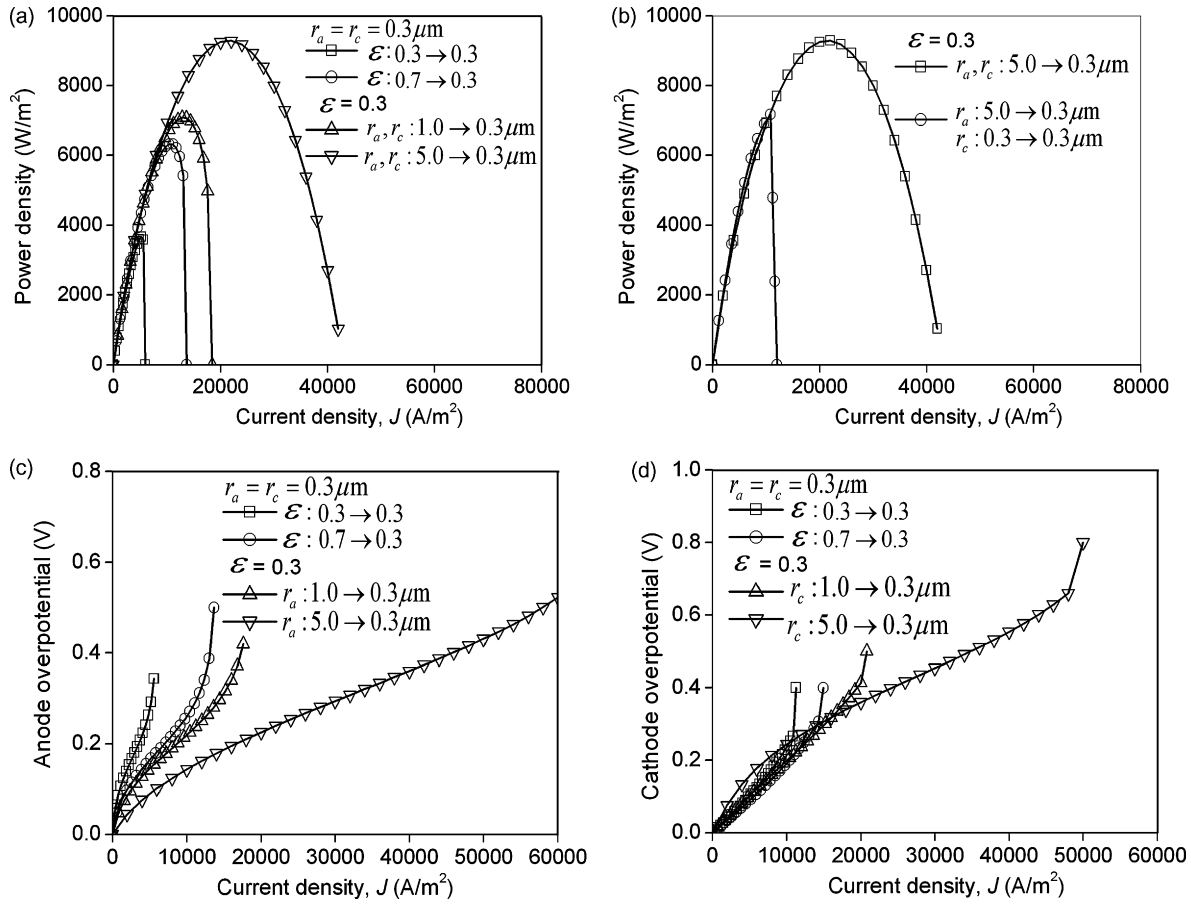

Fig. 9. Comparison of SOFCs with or without FGEs, the particle radius at the EE interface is 0.3 μm: (a) power densities of non-graded SOFC and SOFCs with grading in both electrodes; (b) power densities of SOFC with particle size grading in both electrodes and in one electrode only; (c) anode overpotential; and (d) cathode overpotential.

SOFC performance (compared with only anode-graded SOFC) at medium current density (Fig. 7(b)).

For particle radius of 0.5 μm and 0.3 μm at the EE interface, the performances of SOFC with or without micro-structurally graded electrodes are presented in Figs. 8 and 9, respectively. It is found that the smaller the particle size at the EE interface, the larger the difference between the micro-structurally graded SOFC and the non-graded SOFC (Figs. 8 and 9). For an interfacial particle size of 0.5 μm, the particle size graded SOFC shows significantly higher (as much as 70%) power density than the non-graded SOFC (Fig. 8(a)). In case of particle radius equal to 0.3 μm at the EE interface, the maximum power density of a SOFC with considerable size grading (r: 5.0 μm → 0.3 μm) is 153% higher than that of a non-graded SOFC (Fig. 9(a)). For a non-graded SOFC, decreasing particle size results in considerable increase in the mass transfer resistivity and thus the SOFC power density is low due to the small limiting current density. As mentioned previously, the concentration overpotential is more sensitive to the micro-structural grading than the ohmic and activation overpotentials. Since the gas transport becomes more important for a SOFC with small particle size than one with large particle size, the performance gain is more pronounced for micro-structurally graded SOFC due to the considerably decreased mass transport resistance (Figs. 8(b and c), and 9(c and d). In addition, it can be seen that a large extent of grading of the thin cathode is needed, as illustrated in Fig. 9(b) that a SOFC with both electrodes graded has a higher power density than a SOFC merely with the anode graded.

Compared with porosity grading, particle size grading seems to be more effective to enhance the SOFC performance for small EE interfacial particle size. One reason is that the porosity of the electrodes can only change in a small range (0.3–0.7) due to the limitation of percolation [10,29]. Another reason is that the ohmic overpotential will increase due to grading in porosity. On the contrary, particle size grading does not alter the ohmic overpotential. More importantly, the particle size can be changed in a wider range. As a result, grading in particle size is superior to porosity grading since the current research trend is to make particle size smaller and smaller at the EE interface to enhance the electrode reactivity at an intermediate temperature [8,9,25–27]. In fuel cells and other fields, micro-structurally graded electrodes can be fabricated by a number of ways, such as combustion chemical vapour deposition (CCVD) [8] and electrophoretic deposition [32]. Therefore, the concept of micro-structurally graded SOFC is feasible and has great potential to improve the SOFC performance by simply modifying the electrode microstructures.

5. Conclusion

A mathematical model has been developed to investigate the effect of micro-structural grading on the SOFC performance. The model was validated by comparing the simulation results with experimental data available in the literature. The model is able to analyse the coupled phenomena of electrochemical reactions and mass transfer in the SOFC electrodes.

It is found that both porosity grading and particle size grading are effective to enhance SOFC performance. With a decrease in particle size at the EE interface, the performance gain by particle size grading method becomes more pronounced. It has been demonstrated that the maximum power density of a particle size graded SOFC could be 153% higher than a conventional non-graded SOFC with small particle size, indicating the great promise of micro-structural grading in SOFC. The reason is that the concentration overpotential can be considerably reduced by proper grading of electrode microstructure while the ohmic and activation overpotentials are changed only slightly with micro-structural grading. It is found that the particle size grading becomes more advantageous than porosity grading when the particle size at the EE interface is small. It is also found that the effect of grading is generally beneficial for thick electrodes. However, when the EE interfacial particle size is large, too much grading in particle size of the thin cathode should be avoided for SOFC operating at a low to medium current density.

This paper reveals that micro-structural grading is very promising to enhance the SOFC power density and worthy of further investigation. Aside from their electric performance, other properties associated with micro-structural grading, such as mechanical strength and catalyst sintering, should be further investigated.

Acknowledgement

The work described in this paper was part of an ongoing project supported by a grant from the Research Grants Council of Hong Kong, P.R. China (HKU7150/05E).

References

[1] X.G. Li, Principles of Fuel Cells, Taylor & Francis, New York/London, 2005.
[2] S.C. Singhal, K. Kendall, High Temperature Solid Oxide Fuel Cells—Fundamentals, Design and Applications, Elsevier, New York, 2003.
[3] N. Sammes, Fuel Cell Technology: Reaching Towards Commercialisation, Springer, London, 2006.
[4] J.J. Hwang, C.K. Chen, D.Y. Lai, J. Power Sources 143 (2005) 75–83.
[5] P.A. Ramakrishna, S. Yang, C.H. Sohn, J. Power Sources 158 (2006) 378–384.
[6] Y.H. Koh, J.J. Sun, W.Y. Choi, H.E. Kim, J. Power Sources 161 (2006) 1023–1029.
[7] N.T. Hart, N.P. Brandon, M.J. Day, N. Lapena-Rey, J. Power Sources 106 (2002) 42–50.
[8] Y. Liu, C. Compson, M.L. Liu, J. Power Sources 138 (2004) 194–198.
[9] S.W. Zha, Y.L. Zhang, M.L. Liu, Solid State Ionics 176 (2005) 25–31.
[10] L.C.R. Schneider, C.L. Martin, Y. Bultel, L. Dessemond, D. Bouvard, Electrochim. Acta 52 (2007) 3190–3198.
[11] E.S. Greene, W.K.S. Chiu, M.G. Medeiros, J. Power Sources 161 (2006) 225–231.
[12] S.H. Chan, Z.T. Xia, J. Electrochem. Soc. 148 (2001) A388–A394.
[13] P. Costamagna, P. Costa, V. Antonucci, Electrochim. Acta 43 (1998) 375–394.
[14] M.M. Hussain, X. Li, I. Dincer, J. Power Sources 161 (2006) 1012–1022.
[15] D. Bouvard, F.F. Lange, Acta Metall. Mater. 39 (1991) 3083–3090.
[16] S.H. Chan, Z.T. Xia, J. Appl. Electrochem. 32 (2002) 339–347.
[17] M. Ni, M.K.H. Leung, D.Y.C. Leung, Chem. Eng. Technol. 29 (2006) 636–642.
[18] E. Hernandez-Pacheco, D. Singh, P.N. Hutton, N. Patel, M.D. Mann, J. Power Sources 138 (2004) 174–186.
[19] J.H. Nam, D.H. Jeon, Electrochim. Acta 51 (2006) 3446–3460.
[20] S.H. Chan, K.A. Khor, Z.T. Xia, J. Power Sources 93 (2001) 130–140.
[21] H.Y. Zhu, R.J. Kee, J. Power Sources 117 (2003) 61–74.
[22] S.H. Chan, X.J. Chen, K.A. Khor, J. Electrochem. Soc. 151 (2004) A164–A172.
[23] S.P. Jiang, W. Wang, Y.D. Zhen, J. Power Sources 147 (2005) 1–7.
[24] S.D. Kim, H. Moon, S.H. Hyun, J. Moon, J. Kim, H.W. Lee, Solid State Ionics 177 (2006) 931–938.
[25] M. Brown, S. Prindahl, M. Mogensen, J. Electrochem. Soc. 147 (2000) 475.
[26] S.P. Jiang, P.J. Callus, S.P.S. Badwal, Solid State Ionics 132 (2000) 1–14.
[27] N.P. Bansal, Z.M. Zhong, J. Power Sources 158 (2006) 148–153.
[28] M. Ni, M.K.H. Leung, D.Y.C. Leung, K. Sumathy, Solar Energy Mater. Solar Cells 90 (2006) 1331–1344.
[29] S.J.L. Kang, Sintering: Densification, Grain Growth, and Microstructure, Elsevier/Butterworth-Heineman, Amsterdam, 2004.
[30] D. Bouvard, F.F. Lange, Phys. Rev. A 45 (1992) 5690–5693.
[31] F. Zhao, A.V. Virkar, J. Power Sources 141 (2005) 79–95.
[32] L. Besra, M.L. Liu, Progress Mater. Sci. 52 (2007) 1–61.